MERIS 4th data reprocessing

ATBD 2.24: Vicarious adjustment of the MERIS Ocean Colour radiometry

Ref.: MER4RP-ATBD-2.24

Issue: 2. 0

Date: 28/07/2017

Preparation and signature list

	Name and role	Company	Signature
Prepared by	Nicolas Lamquin and the ACRI-ST team	ACRI-ST	

Distribution List

Company	To
	Public distribution

Change log

Version	Date	Changes
2.0	28/07/2017	Version revised – for the MERIS 4th data reprocessing
1.0	29/09/2011	Initial version – for the MERIS 3rd data reprocessing

Table of Content

ACKNOWLEDGEMENTS ---- **5**

1 INTRODUCTION ---- **6**

1.1 SCOPE OF THE DOCUMENT ---- 6

1.2 ACRONYMS ---- 6

1.3 NOTATIONS ---- 6

2 MOTIVATION TO IMPLEMENT A VICARIOUS ADJUSTMENT ---- **9**

2.1 THEORETICAL LIMITATION OF INSTRUMENTAL CALIBRATION ---- 9

2.2 RECALL OF THE MERIS OCR QUALITY ASSESSEMENT FROM MERIS 2ND DATA REPROCESSING ---- 11

2.3 PRINCIPLE OF THE VICARIOUS ADJUSTMENT FOR MERIS OC RADIOMETRY ---- 13

2.4 DOMAIN OF APPLICABILITY ---- 14

3 IMPLEMENTATION OF THE VICARIOUS ADJUSTMENT IN THE MERIS 4TH DATA REPROCESSING ---- **16**

3.1 OVERVIEW OF THE MERIS 4TH REPROCESSING LEVEL 2 CHAIN ---- 16

3.2 INTERPOLATION SCHEME FOR THE WATER-LEAVING REFLECTANCE ---- 17

3.3 METHODOLOGIES FOR THE VICARIOUS ADJUSTMENT OF THE VISIBLE BANDS ---- 18

3.4 DATA PREPARATION FOR THE VICARIOUS CALIBRATION OF THE VISIBLE BANDS ---- 19

3.4.1 The BOUSSOLE dataset ---- 20

3.4.2 The MOBY dataset ---- 20

3.4.3 Data matching and screening ---- 20

3.4.4 Correction of downwelling sun irradiance for the in situ water-leaving reflectance ---- 21

3.4.5 Denormalization procedure for the in situ water-leaving reflectance ---- 21

3.5 VICARIOUS GAINS COMPUTATION ---- 21

3.6 VALIDATION ON MERMAID MATCHUPS ---- 24

4 REFERENCES ---- **28**

List of Figures

Figure 1: Example of relative contribution of the marine signal to the total signal, $\boldsymbol{td\lambda\rho w\lambda/\rho gc\lambda}$, for MERIS acquisitions over different type of waters: AAOT (Adriatic Sea), MOBY (Pacific Ocean) and BOUSSOLE (Mediterranean Sea). 10

Figure 2: Relative errors of MERIS 2nd reprocessing rhow on the MERMAID dataset. Matchups are constructed on 5x5 RR pixels window with less than 50% pixels flagged by Cloud or Ice_haze or High_glint or Medium_glint or PCD_1_13 or PCD_19. 12

Figure 3: Vicarious gains computed over BOUSSOLE, MOBY, and final gains for MERIS 4th data reprocessing. Dashed lined represent standard deviation. 23

Figure 4: Final vicarious gains computed independently for selected pressure levels 1040, 1013.25, 970 hPa, compared to the nominal set of gains (dashed). 24

Figure 5: Relative percent difference in water-leaving reflectance between in situ and satellite (MERMAID) for wavebands 412, 443, 490 nm. From top to bottom: 2nd, 3rd, and 4th data reprocessings 25

Figure 6: Relative percent difference in water-leaving reflectance between in situ and satellite (MERMAID) for wavebands 510, 560, 665 nm. From top to bottom: 2nd, 3rd, and 4th reprocessings... 26

Figure 7: Difference in water-leaving reflectance between in situ and MERIS 4th reprocessing (MERMAID) for waveband 412 nm. Left: individual gain formulation (15), right: formulation (14). ... 27

List of Tables

Table 1: Averaged gains per site and number of matchups, Final gains and standard deviation..... 22

Acknowledgements

We gratefully acknowledge the following Principle Investigators who contribute to MERMAID (http://mermaid.acri.fr) and provide extremely valuable in situ data:

- Giuseppe Zibordi (Joint Research Center, Italy) for providing data at five AERONET- OC sites (the Acqua Alta Oceanographic Tower, Abu Al Bukhoosh, Gloria, Gustav Dalen Tower and Helsinki Lighthouse (Zibordi *et al.,* 2009a, Zibordi *et al.,* 2009b)) as well as data from the BioOptEuroFleets (Jean-Francois Berthon, and Elisabetta Canuti also thanked for these ones).
- Greg Schuster for providing data at the AERONET- OC site CoveSeaPRISM.
- Alex Gilerson and Sam Ahmed for providing data at the AERONET- OC site LISCO.
- Alan Weidemann, Bill Gibson, and Robert Arnone for providing data at the AERONET- OC site WaveCIS.
- John Icely (University of Algarve, Portugal) for the Sagres coast dataset (Cristina *et al.,* 2009).
- David Antoine (Laboratoire d'Océanographie de Villefranche, France) for the BOUSSOLE dataset, used in particular for the vicarious adjustment (Antoine *et al.,* 2006, Antoine *et al.,* 2008a).
- David McKee (University of Strathclyde, UK) for the Bristol Channel and Irish Sea datasets.
- Mati Kahru (University of California, US) for the California Current dataset.
- Hubert Loisel (Laboratoire d'Océanologie et de Géosciences, France) for the East English Channel and French Guiana datasets (Loisel *et al.,* 2007, Lubac and Loisel, 2007).
- Michael Ondrusek (NOAA) for the MOBY dataset used for the vicarious adjustment (Clark *et al.,* 2003).
- Kevin Ruddick (MUMM, Belgium) for the MUMMTriOS dataset (Ruddick *et al.,* 2006).
- Doug Vandemark and Hui Feng (University of New Hampshire, US) for the AERONET-OC MVCO dataset (Zibordi *et al.,* 2009).
- Jeremy Werdell (NASA), Larry Harding (University of Maryland, US), Antonio Mannino (NASA), Ajit Subramaniam (University of Maryland, US), Dariusz Stramski (University of California, US), Greg Mitchell (University of California, US), William Balch (Bigelow Laboratory for Ocean Sciences, US), Frank Muller-Karger (University South Florida, US), Ru Morrison (Woods Hole Oceanographic Institution, US), Zhongping Lee (Naval Research Laboratory), Ken Carder (Professor Emeritus University South Florida, US), Norman Nelson (University of California, US), Richard Gould (Naval Research Laboratory, US), Robert Arnone (Naval Research Laboratory, US) and Stan Hooker (NASA) for the NOMAD dataset (Werdell and Bailey, 2005).
- Suzanne Kratzer (University of Stockholm, Sweden) for the North-Western Baltic Sea and AERONET-OC Palgrunden dataset (Kratzer *et al.,* 2008).
- David Siegel (University of California, US) for the Plumes and Blooms dataset.
- Pierre-Yves Deschamps (Laboratoire d'Optique Appliquée, France) for the SIMBADA dataset.
- Annelies Hommersom (IVM, Netherlands) for the Wadden Sea dataset.

1 Introduction

1.1 Scope of the document

This Algorithm Theoretical Basis Document 2.24 describes the vicarious adjustment of the MERIS ocean colour radiometry implemented in the Level 2 processing chain for the 4th data reprocessing.

It presents the evolution of the method from its first implementation for the MERIS 3rd data reprocessing (MERIS ATBD 2.24, issued on Sep 2011), its validation against *in situ* data and provides the adjustment factors used in the 4th reprocessing configuration and available in the nominal configuration of the ODESA processor.

1.2 Acronyms

The definition of the acronyms used in this document is provided below.

Acronym	Definition
AAOT	Acqua-Alta Oceanographic Tower
AERONET-OC	AEosol RObotic NETwork – Ocean Color
ATBD	Algorithm Theoretical Basis Document
BOUSSOLE	BOUée pour l'acquiSition de Séries Optiques à Long termE
BPAC	Bright Pixel Atmospheric Correction
CCD	Charged-Coupled Device
ESA	European Space Agency
LUT	Look-Up Table
MERIS	MEdium Range Imaging Spectrometer
MERMAID	MERIS Matchup In Situ Database
MOBY	Marine Optical BuoY
MODIS	Moderate Resolution Imaging Spectroradiometer
NIR	Near Infra-Red
NOMAD	NASA bio-Optical Marine Algorithm Dataset
OCR	Ocean Colour Radiometry
ODESA	Optical Data processor of ESA
QWG	Quality Working Group
RR	Reduced Resolution
SeaWiFS	Sea-viewing Wide Field-of-view Sensor
TOA	Top Of Atmosphere
VIS	Visible part of the spectrum

1.3 Notations

The definition of the notations used in this document is provided below.

Symbol	Definition	Dimension/Units
λ	Wavelength	nm, also used as index
λ_{NIR}	NIR wavelength	nm, also used as index
i	Index for a target measurement (location and time)	Dimensionless
P_{std}	Reference pressure level for the radiative transfer simulations	hPa, also used as index
P_1, P_2	Closest and bracketing reference pressure levels	hPa, also used as indices
P_{pix}	Pixel pressure	hPa
$L_{TOA}(\lambda)$	Level 1 TOA radiance	$mW.m^{-2}.nm^{-1}.sr^{-1}$
$L_w(\lambda)$	Level 2 water-leaving radiance	$mW.m^{-2}.nm^{-1}.sr^{-1}$
$\rho_{TOA}(\lambda)$	TOA reflectance	Dimensionless
$\rho_{ng}(\lambda)$	TOA reflectance corrected for gaseous absorption	Dimensionless
$t_g(\lambda)$	Total gaseous transmittance	Dimensionless
$t\rho_g(\lambda)$	Glint reflectance at TOA level	Dimensionless
$\rho_{gc}(\lambda)$	TOA reflectance corrected for gaseous absorption and glint	Dimensionless
$\rho_{gc}^{t}(\lambda)$	Targeted “all”-corrected reflectance	Dimensionless
$\rho_{gc}^{*}(\lambda)$	TOA reflectance corrected for gaseous absorption, glint, smile, Bodhaine latitudinal dependency of Rayleigh optical thickness, and pressure (“all”-corrected)	Dimensionless
$\rho_{gc}^{*,IS}(\lambda)$	Same as above but for in situ	Dimensionless
$\rho_{path}(\lambda)$	Atmospheric path reflectance	Dimensionless
$\rho_R(\lambda)$	Rayleigh reflectance	Dimensionless
$\tau_R(\lambda)$	Rayleigh optical thickness	m^{-1}
$\rho_{aer}(\lambda)$	Aerosol reflectance	Dimensionless
$\rho_w(\lambda)$	Water-leaving reflectance	Dimensionless
$\rho_w^{IS}(\lambda)$	In situ water-leaving reflectance	Dimensionless
$E_s(\lambda)$	In situ, measured, solar irradiance	$mW.m^{-2}.nm^{-1}$
$E_s^{ME}(\lambda)$	In situ, MERIS-normalized, solar irradiance	$mW.m^{-2}.nm^{-1}$
$\rho_w^{ISME}(\lambda)$	In situ water-leaving reflectance, normalized to MERIS solar irradiance	Dimensionless
$t_d(\lambda)$	Total (direct and diffuse) transmittance	Dimensionless
$t\rho_{wC2(\lambda)}$	TOA water-leaving reflectance retrieved by the Bright Pixel Atmospheric Correction at 709, 779, 865 and 885 nm	Dimensionless
$g(\lambda)$	Individual adjustment factor per macropixel	Dimensionless

$\sigma_g(\lambda)$	Total uncertainty on individual adjustment factor per macropixel	Dimensionless
$\sigma_g^{IS}(\lambda)$	In situ uncertainty component of individual adjustment factor per macropixel	Dimensionless
$\sigma_g^{ME}(\lambda)$	MERIS uncertainty component of individual adjustment factor per macropixel	Dimensionless
$\omega(\lambda)$	Weight of individual adjustment factor	Dimensionless
$G(\lambda)$	Weighted-mean adjustment factor	Dimensionless
θ_s	Sun zenith angle	Degree
θ_v	View zenith angle	Degree
$\Delta\varphi$	Relative azimuth angle	Degree

2 Motivation to implement a vicarious adjustment

2.1 Theoretical limitation of instrumental calibration

The primary aim of Ocean Colour Radiometry (OCR) space born sensors such as MERIS is to retrieve the water-leaving signal at sea level from a Top-Of-Atmosphere (TOA) optical measurement, over the Visible (VIS) and Near-InfraRed (NIR) spectral domain.

The signal at ocean surface can be either expressed in term of radiance (energy) $L_w(\lambda)$ or reflectance (ratio to downwelling Solar irradiance) $\rho_w(\lambda)$, where λ is the wavelength. Hereinafter, we shall only consider the water-leaving reflectance ρ_w notation, used in the MERIS data distribution context since 2002 (Rast and Bezy, 1999) and used more recently for MODIS and SeaWiFS (see *e.g.* http://oceancolor.gsfc.nasa.gov/reprocessing/).

The expected accuracy on $\rho_w(\lambda)$ is mainly governed by further exploitation of the signal, for instance to assess marine constituents concentration or other bio-optical quantities (*e.g.* chlorophyll-a, suspended matter, diffuse attenuation coefficient, transparency, etc.) by spectral inversion. In this document we shall rely on the only few specifications derived in the past, essentially designed for quantifying chlorophyll-a in the open ocean. A typical order of relative accuracy is 5% in the blue-green spectral region (Gordon, 1997). More recently, for the MERIS mission, the goal of discriminating ten classes of chlorophyll concentration within each of the three orders of magnitude between 0.03, 0.3, 3 and 30 mg/m^3 leads to a requirement of about ±1-2.10^{-3} absolute accuracy at 443 nm and ±5.10^{-4} at 560 nm, using a band ratio algorithm (Antoine and Morel, 1999).

Actual accuracy of remotely-sensed ρ_w depends mainly on the quality of both TOA acquisition (*i.e.* quality of the absolute and interband sensor calibration) and the atmospheric correction (*i.e.* ability to estimate and remove the atmospheric path contribution, see *e.g.* Antoine and Morel, 1998). This can be made explicit by the following schematic decomposition of the signal, in ideal conditions without sun specular reflection or white caps, and after correction of atmospheric gas absorption (see symbols definition in § 1.3):

$$\rho_{gc}(\lambda) = \rho_{path}(\lambda) + t_d(\lambda).\rho_w(\lambda) \qquad (1)$$

The ρ_{gc} quantity will be described more precisely latter in the MERIS context, and can be understood, at this stage, as the TOA reflectance ρ_{TOA} processed up to the atmospheric correction.

Most of the current operational atmospheric correction algorithms consist in first, assessing the aerosol optical properties from the NIR bands; then, propagating the path reflectance $\rho_{path}(\lambda)$ and total (direct and diffuse) transmittance $t_d(\lambda)$ at any wavelength λ in the visible; and finally, deducing the marine signal by inversing equation (1) (see Antoine and Morel, 1999, for MERIS, and Gordon and Wang, 1994, for SeaWiFS). Hence, whatever the accuracy of the path reflectance retrieval, any error $\Delta\rho_{gc}$ on the total signal implies an error $\Delta\rho_w$ on the marine reflectance of:

$$\frac{\Delta\rho_w(\lambda)}{\rho_w(\lambda)} = \frac{\Delta\rho_{gc}(\lambda)}{\rho_{gc}(\lambda)} \Big/ \frac{t_d(\lambda).\rho_w(\lambda)}{\rho_{gc}(\lambda)} \qquad (2)$$

The denominator on the right-hand side represents the relative contribution of the marine reflectance at TOA level to the total signal and typically lies between 5% and 20%, depending on the wavelengths and type of water (see figure below). This means that reaching a 5% accuracy on ρ_w requires an absolute accuracy on ρ_{gc} (hence on ρ_{TOA}) between 0.25% and 1%, which cannot be insured through purely instrumental calibration and characterisation (Gordon, 1998).

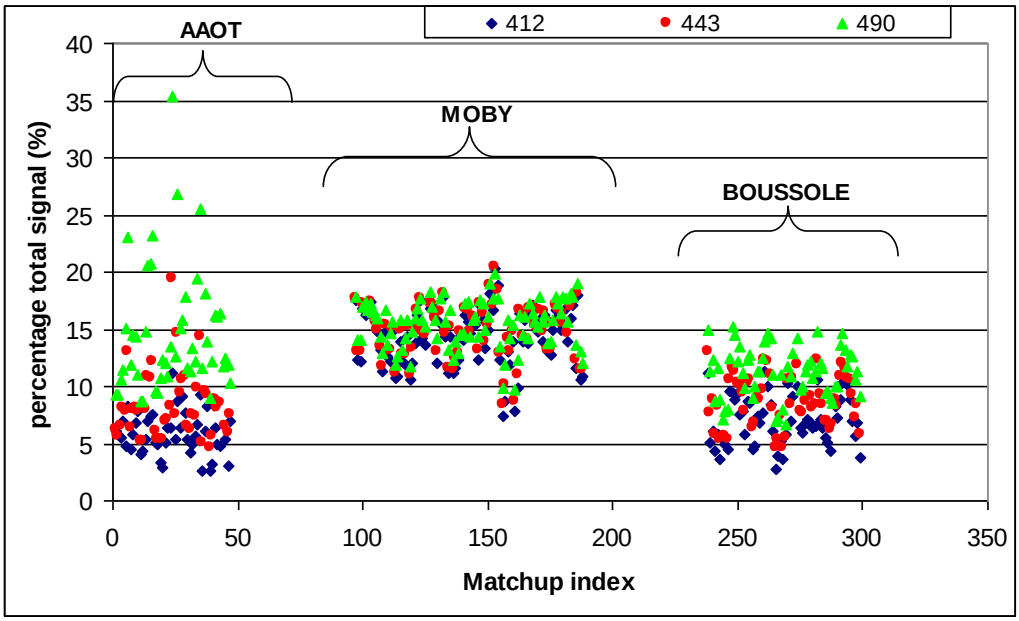

Figure 1: Example of relative contribution of the marine signal to the total signal, $t_d(\lambda)\rho_w(\lambda)/\rho_{gc}(\lambda)$, for MERIS acquisitions over different type of waters: AAOT (Adriatic Sea), MOBY (Pacific Ocean) and BOUSSOLE (Mediterranean Sea).

For instance, first MERIS calibration and validation showed that the *in situ* estimations of TOA radiances lie within less than 6% of the measurement (Kneubühler, 2002). Regarding SeaWiFS, pre-launch calibration uncertainties are approximately 3% of the TOA radiance (Eplee *et al.*, 2001).

2.2 Recall of the MERIS OCR quality assessement from MERIS 2nd data reprocessing

Several independent validation exercises conducted in the past have proven significant positive bias in the MERIS 2nd reprocessing water leaving reflectance. For instance, Antoine *et al.* (2008b) have quantified over the BOUSSOLE buoys relative percentage difference of about 60% at 412 nm, 30% at 443 nm, 15% at 490 nm and 20% at 510 and 560 nm. Zibordi *et al.* (2006) found also values between 15% and 42% in the 443-560 nm spectral range at the AAOT site.

In parallel with the MERIS 3rd reprocessing activities, the MERMAID matchup system has been settled in collaboration with *in situ* data providers in order to get a significant number of validation points with controlled quality. It constitutes a central tool in the present work, with more than 20 *in situ* datasets (fixed stations or cruises, including the NOMAD dataset described in Werdell and Bailey, 2005) associated to MERIS data extractions. Details on the optical measurements protocols and matchup facility are available on the website http://mermaid.acri.fr. The quality assessment of the MERIS 2nd reprocessing on the MERMAID matchups confirms globaly a large overestimation in the water-leaving reflectance, of few tens of percents (see histograms in Figure *2*). It is especially true for clear or moderately turbid waters (MOBY, BOUSSOLE, AAOT), while more turbid waters (part of the SIMBADA cruise, Plumes & Blooms…) show negative bias. This difference between both kinds of waters may come from the atmospheric correction over bright pixel in the NIR.

Matching the required 5% uncertainty on the water-leaving radiometry is thus not met with the standard MERIS 2nd reprocessing, and, more generally, is agreed to be particularly difficult for any sensor (see *e.g.* Hooker *et al,* 1992, Hooker and McClain, 2000 for SeaWiFS). This has lead NASA to rely on vicarious calibration since few decades (from SeaWiFS onwards), that is on a complementary calibration using ground-truth measurements (see Franz *et al.* 2001, Franz *et al.* 2007; Bailey *et al.* 2008 for recent methodologies and results).

Following the recommendation of the works cited above, the MERIS Quality Working Group has decided to consider a vicarious methodology for the 3rd MERIS data reprocessing.

This methodology has been adapted to the algorithmic evolutions of the 4th MERIS data reprocessing, which is the point adressed in this document.

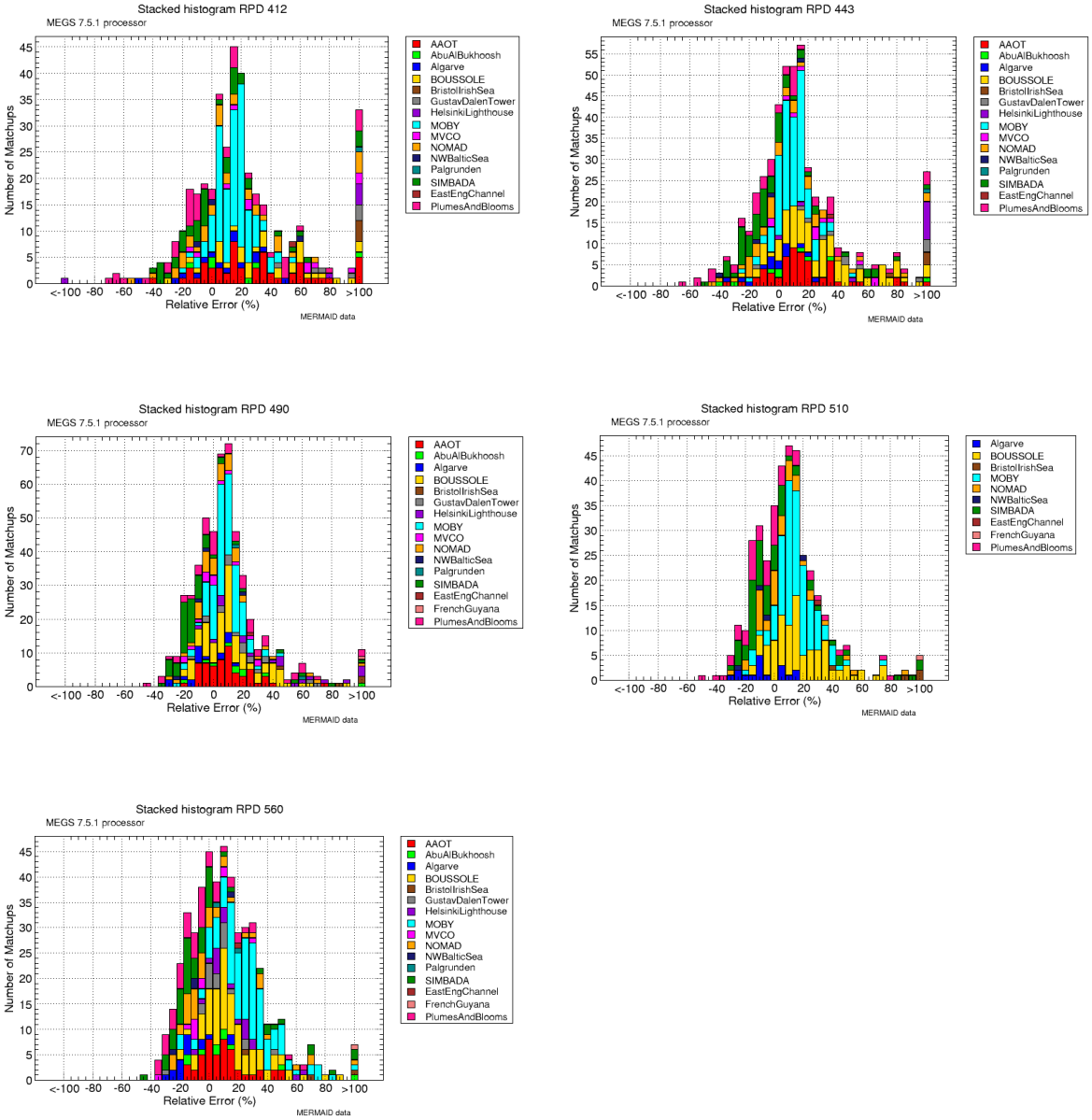

Figure 2: Relative errors of MERIS 2nd reprocessing rhow on the MERMAID dataset. Matchups are constructed on 5x5 RR pixels window with less than 50% pixels flagged by Cloud or Ice_haze or High_glint or Medium_glint or PCD_1_13 or PCD_19.

2.3 Principle of the vicarious adjustment for MERIS OC radiometry

In this document it is chosen to use the terminology of a vicarious *adjustment*, rather than *calibration* as in the seminal work on the NASA sensors (*e.g.* Gordon, 1997, Franz *et al.,* 2001), because our purpose is to adjust internaly the Level 2 Ocean branch processing and not to modify the Level 1 TOA radiometric calibration. Hence it is worth noting that the Level 1 products of the 4th MERIS data reprocessing are not vicariously calibrated.

The primary idea of the vicarious adjustment is to consider that errors in water-leaving reflectance come from a systematic bias at TOA, which can be assessed by comparison to reference or *targeted* reflectance ρ_{gc}^{t} on a trustworthy dataset of observations. We recall here that ρ_{gc} is equivalent to ρ_{TOA} after some pre-corrections and outside the sun glint (or after correction for it). This problem might come either from an actual bias in the radiometric calibration of the sensor or from inaccuracy of the atmospheric correction based on a radiative transfer modelling. The vicarious adjustment aims at solving blindly the bias issue whatever its exact origin.

For a given target in space and time, hereafter indexed by *i*, the comparison between the ground truth signal ρ_{gc}^{t} and the measured reflectance ρ_{gc} leads to a local adjustment factor defined by:

$$g(\lambda, i) = \frac{\rho_{gc}^{t}(\lambda, i)}{\rho_{gc}(\lambda, i)} \qquad (3)$$

Provided a statistically representative amount of targets, N, and homogeneous individual factors $g(\lambda, i)$, a reliable average gain can then be calculated using a weighted average:

$$G(\lambda) = \frac{\sum_{i=1}^{N} \omega(\lambda, i) g(\lambda, i)}{\sum_{i=1}^{N} \omega(\lambda, i)} \qquad (4)$$

Where weights are, for instance, the inverse of the uncertainty of each individual gains determined from the sampling standard deviation of MERIS data as well as in situ uncertainty. This means that we give more credence in the least uncertain individual gains.

Once determined, this gain is systematically applied in operation as a multiplicative factor to the measured TOA reflectance $\rho_{gc}(\lambda)$, just before the atmospheric correction step.

It is important to notice that a single set of spectral gains is applied throughout the entire mission and whatever the camera and CCD detector in the field of view. Hence homogeneity in the individual factors $g(\lambda, i)$ should ensure a robust vicarious calibration.

The targeted reflectance ρ_{gc}^{t} required in the gain computation would ideally be built from concomitant ground measurements of water leaving reflectance, atmospheric aerosol reflectance and atmospheric diffuse transmittance. While reliable *in situ* water leaving reflectances ρ_{w}^{IS} are accessible, simultaneous measurements with aerosol properties are not widely available (Franz *et al.*, 2001). To sort out this lack of *in situ* measurements, published procedures have proposed to use the atmospheric variables determined algorithmically by

the atmospheric correction above the marine target, after insuring a proper calibration of the NIR bands (Franz *et al.,* 2007, Bailey *et al.,* 2008). This means a two-step procedure:

1. First, the NIR bands used in the atmospheric correction, 779 and 865 nm, are independently adjusted, if necessary;
2. Then, the atmospheric correction is applied, yielding to path reflectance and transmittance in the VIS bands considered as sufficiently accurate to build the targeted TOA reflectance:

$$\rho_{gc}^{t}(\lambda,i) = \rho_{path}^{vic}(\lambda,i) + t_{d}^{vic}(\lambda,i).\rho_{w}^{IS}(\lambda,i) \qquad (5)$$

where the exponent ^{vic} stands for vicariously adjusted quantities.

An advantage of this approach, pointed out in the first works of NASA, is to decouple the NIR and VIS gains computation and avoid a complex iterative procedure.

Without further atmospheric *in situ* measurement, the first step needs assumptions on the aerosol signal in the NIR. This can be either by fixing an aerosol model already tabulated in the ground segment (*e.g.* Franz *et al.,* 2007), or by making an assumption on the spectral shape, which was done for the MERIS 3rd data reprocessing.

In the MERIS 4th data reprocessing NIR adjustment is performed through an evolution of the BPAC algorithm (MERIS ATBD 2.6). Whether the water is considered turbid or clear a spectral alignment is made on the NIR signal to fit the shape of the aerosol models used in the BPAC. Residual terms from the alignment, if not coming from turbid water contributions, are considered as NIR calibration residuals. At the end, both turbid water signature in the NIR and NIR calibration are removed to the TOA reflectances in order to provide the dark water inputs of the Antoine and Morel (1999) atmospheric correction. By construction, applying the individual gain $g(\lambda,i)$ would locally make the atmospheric correction perfectly retrieve the desired *in situ* reflectance $\rho_{w}^{IS}(\lambda,i)$, whatever the NIR adjustment. This is not true in practice since only an average adjustment factor $G(\lambda)$ is applied. Hopefully the near infrared adjustment may tend to improve accuracy of the atmospheric correction and consequently reduce dispersion in the visible gain factors.

2.4 Domain of applicability

The primary unknown in $\rho_{gc}^{t}(\lambda)$ being the water-leaving reflectance and the aerosol reflectance (see *e.g.* equation 5), we have decided to put ourselves in situation of stable and homogeneous marine and aerosol properties, *i.e.* avoid coastal areas to weaken the influence of highly variable and complex waters and assemblage of aerosol particles.

In addition, and despite the importance to monitor coastal regions, the objective of vicarious adjustment is to improve remote-sensing of the widest possible areas of the oceans: open ocean areas dominated by phytoplankton optical properties. For these reasons, computation of the vicarious adjustment gains has been performed on clear oceanic waters. The application of those gains will obviously present some limitations in coastal waters. We indeed extended

our work and computed vicarious gains on more coastal datasets (mainly AERONET-OC sites; http://aeronet.gsfc.nasa.gov, Holben et al., 1998). In coastal regions, the spectral gains proved to present opposite trends in comparison to open ocean derived ones. These results are confirmed by the work of Melin and Zibordi (2010).

3 Implementation of the vicarious adjustment in the MERIS 4th data reprocessing

3.1 Overview of the MERIS 4th reprocessing Level 2 chain

We give here an overview of the Level 2 processing chain and detail where the vicarious adjustment has been inserted. Depency on the geometrical angles θ_s, θ_v and $\Delta\varphi$ is not made explicit.

One major evolution of the MERIS 4th data reprocessing ocean branch is the pressure adjustment scheme that adjusts the TOA signal to the signal that would be acquired if the target pressure were fixed to a standard pressure. This scheme must be applied to cope with the radiative transfer modeling of the atmospheric signal at fixed standard pressure levels.

In the MERIS 3rd data reprocessing, this adjustment took place on the path reflectance just prior to the selection of the aerosol models in the Antoine and Morel (1999) atmospheric correction scheme.

In the MERIS 4th data reprocessing, decision of the MERIS QWG has been to adjust the TOA signal to the standard pressure just after the gaseous transmission and glint corrections. The rationale is to consider at the same time the dependency of the Rayleigh optical thickness with latitude (so-called Bodhaine correction (Santer and Zagolski, 2017)), the smile correction (wavelength-shift induced correction), and the pressure adjustment. The adjustment is done using an equivalent Rayleigh optical thickness shift following the 6S theoretical formulation of the signal.

MERIS Level 1 products correspond to geolocated and calibrated TOA radiances $L_{TOA}(\lambda)$. The Level 2 chain starts by converting the Level 1 data into TOA reflectances $\rho_{TOA}(\lambda)$. Then, several processings are sequentially applied, at a pixel level:

- a pixel identification allowing to flag Cloud, Water and Land pixels and guide the next processing steps into the corresponding branches
- a correction of the total gaseous absorption for O_3, O_2, NO_2,and H_2O, leading to $\rho_{ng}(\lambda)$ related to $\rho_{TOA}(\lambda)$ through:

$$\rho_{TOA}(\lambda) = t_g(\lambda).\rho_{ng}(\lambda) \qquad (6)$$

- a glint correction removing the glint reflectance estimated at sea level by the Cox and Munck (1954) model and propagated at TOA by a simplified transmittance $t(\lambda)$ (see Cox and Munk, 1954, and MERIS ATBD 2.13) depending only in the Rayleigh optical thickness. This correction leads to the glint-corrected reflectance $\rho_{gc}(\lambda)$ related to $\rho_{ng}(\lambda)$ through:

$$\rho_{ng}(\lambda) = \rho_{gc}(\lambda) + t(\lambda).\rho_g(\lambda) \qquad (7)$$

- the smile, Bodhaine, and pressure adjustment (see Santer and Zagolski 2017 for details) reducing the in-field of view variation of channels central wavelengths, correcting for the

latitudinal dependency of the Rayleigh optical thickness, and adjusting the signal to P_{std}, the standard pressure of the radiative transfer look-up-tables (LUTs):

$$\rho_{gc}(\lambda) \rightarrow \rho_{gc}^{*}(\lambda, P_{std}) \qquad (8)$$

- the BPAC removing turbid water contributions to the TOA signal as well as NIR calibration residuals in the NIR only:

$$\rho_{path}(\lambda_{NIR}, P_{std}) = \rho_{gc}^{*}(\lambda_{NIR}, P_{std}) - t\rho_{wC2}(\lambda_{NIR}, P_{std}) \qquad (9)$$

- the Antoine and Morel atmospheric correction estimating the atmospheric path reflectance and the transmittance related to combined aerosols and Rayleigh effects in the VIS from the NIR

$$\rho_{path}(\lambda_{NIR}, P_{std}) \rightarrow \rho_{path}(\lambda, P_{std}) \text{ and } t_d(\lambda, P_{std}) \qquad (10)$$

- at this stage these "all"-corrected reflectances can be related to the water pixels by:

$$\rho_{gc}^{*}(\lambda, P_{std}) = \rho_{path}(\lambda, P_{std}) + t_d(\lambda, P_{std}).\rho_w(\lambda) \qquad (11)$$

The atmospheric path reflectance $\rho_{path}(\lambda, P_{std})$ and the total transmittance $t_d(\lambda, P_{std})$ are given the dependency on P_{std} which is implicit through their computation but is important to mention for the following. Note that there is no white-caps correction in the MERIS processing. Once the spectrum $\rho_w(\lambda)$ is retrieved, the further steps of the Level 2 chain deal with bio-optical inversions.

3.2 Interpolation scheme for the water-leaving reflectance

In the formulation of $\rho_{gc}^{*}(\lambda, P_{std})$ there is no pressure dependency of the water-leaving reflectance $\rho_w(\lambda)$ because it is not dependent on the atmospheric state. It means that any value P_{std} used for simulating the atmospheric state must, in principle, lead to the same results.

This is not completely true in practice as the pressure (or so-called "Rayleigh") adjustment is more efficient for small deviations (i.e. when applied using the LUT reference pressure closest to the target geophysical pressure). For MERIS 4th reprocessing specific radiative transfer simulations have been run to deal with high altitude (low pressure) water bodies, the series of LUTs representing the atmospheric state now includes the dependency in P_{std} so that $P_{std} \in \{1040, 1013.25, 970, 900, 800, 700\}$ hPa where it used to be only $P_{std} = 1013.25$ hPa.

An analysis has been conducted to assess the sensitivity of $\rho_w(\lambda)$ to a change in P_{std}. It appeared that a better precision on $\rho_w(\lambda)$ is obtained if the atmospheric correction is made on the two closest pressure levels of the LUTs and then interpolated.

Let P_1 and P_2 be the pressure levels (one of the six levels available) bracketing the target pressure P_{pix}, P_1 being the closest to P_{pix}.

Mathematically we have:

$$\rho_{gc}^*(\lambda, P_1) = \rho_{path}(\lambda, P_1) + t_d(\lambda, P_1).\rho_w(\lambda, P_1) \qquad (12a)$$

and

$$\rho_{gc}^*(\lambda, P_2) = \rho_{path}(\lambda, P_2) + t_d(\lambda, P_2).\rho_w(\lambda, P_2) \qquad (12b)$$

The Antoine and Morel (1999) atmospheric scheme is performed only at P_1 to retrieve the aerosol models and mixing ratio (see below for explanations). These are later propagated to P_2 through interpolation in the LUTs.

Because the pressure adjustment scheme relies on the Rayleigh optical thickness, the interpolation of $\rho_w(\lambda, P_1)$ and $\rho_w(\lambda, P_2)$ is performed using the corresponding Rayleigh optical thicknesses, namely $\tau_R(\lambda, P_1)$, $\tau_R(\lambda, P_2)$, and $\tau_R(\lambda, P_{pix})$.

Defining $(\lambda) = \frac{\tau_R(\lambda,P_1)-\tau_R(\lambda,P_{pix})}{\tau_R(\lambda,P_1)-\tau_R(\lambda,P_2)}$, we have

$$\rho_w(\lambda) = \big(1 - \epsilon(\lambda)\big).\rho_w(\lambda, P_1) + \epsilon(\lambda).\rho_w(\lambda, P_2) \qquad (13)$$

3.3 Methodologies for the vicarious adjustment of the visible bands

We recall that the NIR bands are supposed to be adjusted within the MERIS 4th reprocessing BPAC, residual spectral alignment of the NIR bands is transferred in the turbid correction term $t\rho_{wC2}(\lambda_{NIR}, P_1)$ which is removed to the "all"-corrected reflectance prior to atmospheric correction. The aerosol loading (AOT, angström exponent, selected aerosol models and mixing ratio) is thus determined from the signal adjusted at P_1 using $\rho_{path}(\lambda_{NIR}, P_1) = \rho_{gc}^*(\lambda_{NIR}, P_1) - t\rho_{wC2}(\lambda_{NIR}, P_1)$.

The aerosol loading is supposed independent of the choice of P_{std}, it is in second step used to get the atmospheric path reflectances and transmittances at both P_1 and P_2 at all wavelengths.

As a NIR spectral alignment is performed through the BPAC, only the visible bands need a proper vicarious calibration. To do so one must relate the in-situ water-leaving reflectances $\rho_w^{IS}(\lambda, i)$ to the "all"-corrected reflectances $\rho_{gc}^*(\lambda, P_1)$ and $\rho_{gc}^*(\lambda, P_2)$, or going backwards into the pressure adjustment scheme to relate these to the sole glint-corrected reflectances $\rho_{gc}(\lambda)$ which is less straightforward.

That is now a slight change compared to equation (3) proposed for MERIS 3rd reprocessing. Two solutions have been proposed by MERIS QWG, leading to equivalent results, to apply vicarious gains on $\rho^*_{gc}(\lambda, P_1)$ and $\rho^*_{gc}(\lambda, P_2)$:

1. Compute vicarious gains independently for each P_{std} branch, i.e. force the processing to not interpolate between two branches so that only one branch is used for adjustments and atmospheric correction, then compute gains for each of the six branches. In the nominal processing two different sets of vicarious gains would then be applied to $\rho^*_{gc}(\lambda, P_1)$ and $\rho^*_{gc}(\lambda, P_2)$ respectively.
2. Compute one unique set of vicarious gains to apply on both $\rho^*_{gc}(\lambda, P_1)$ and $\rho^*_{gc}(\lambda, P_2)$.

On an individual basis (i.e. on each matchup between in-situ measurements and MERIS acquisitions) this leads to solve per wavelength:

1. $g(\lambda, i, P_{std}) = \frac{\rho^{*,IS}_{gc}(\lambda,i,P_{std})}{\rho^*_{gc}(\lambda,i,P_{std})} = \frac{\rho_{path}(\lambda,i,P_{std})+t_d(\lambda,i,P_{std})\rho^{IS}_w(\lambda,i)}{\rho_{path}(\lambda,i,P_{std})+t_d(\lambda,i,P_{std})\rho_w(\lambda,i)}$ for each P_{std} (14)
2. find $g(\lambda, i)$ independently of bracketing pressures P_1 and P_2 so that

$$g(\lambda,i)\rho^*_{gc}(\lambda,i,P_{1-2}) = \rho_{path}(\lambda,i,P_{1-2}) + t_d(\lambda,i,P_{1-2})\rho^{IS}_w(\lambda,i)$$

Because one wants $\rho^{IS}_w(\lambda,i) = \big(1 - \epsilon(\lambda,i)\big).\rho_w\big(\lambda,P_1\big) + \epsilon(\lambda,i).\rho_w\big(\lambda,P_2\big)$, injecting the formulations (9a) and (9b) in both P_1 and P_2 branches leads to solve

$$g(\lambda,i) = \frac{\rho^{IS}_w(\lambda,i) + \big(1 - \epsilon(\lambda,i)\big).\frac{\rho_{path}(\lambda,P_1)}{t_d(\lambda,P_1)} + \epsilon(\lambda,i).\frac{\rho_{path}(\lambda,P_2)}{t_d(\lambda,P_2)}}{\big(1 - \epsilon(\lambda,i)\big).\frac{\rho^*_{gc}(\lambda,P_1)}{t_d(\lambda,P_1)} + \epsilon(\lambda,i).\frac{\rho^*_{gc}(\lambda,P_2)}{t_d(\lambda,P_2)}} \quad (15)$$

The implementation of the second choice was decided as it is the simplest and the closest to the implementation for MERIS 3rd reprocessing. However, question remains on the proper computation and validation of vicarious gains dedicated to high altitude water bodies.

3.4 Data preparation for the vicarious calibration of the visible bands

For reasons already mentioned in section 2.4, the in situ datasets for vicarious adjustment have been selected with respect to their representativeness of world ocean Case 1 waters. We have chosen the MOBY (Clark et al., 2003) and BOUSSOLE (Antoine et al., 2006, Antoine et al., 2008a) buoys for they provide the longest time series of quality checked data in such conditions. Matchups extractions were made from the MERMAID system available at http://mermaid.acri.fr. A reason to consider two sites is to dispose of the maximum of reference optical measurements. As we shall see hereafter, this approach is a posteriori validated thanks to a good consistency in the gain factors from the two sites.

3.4.1 The BOUSSOLE dataset

The BOUSSOLE mooring (BOUée pour l'acquiSition de Séries Optiques à Long termE) is in operation since 2003 and located in the Ligurian Sea (Western Mediteranean – 7°54'E, 43°22'N, depth of 2440m). Oligotrophic conditions prevail during summer with Chl-a ranging within 0.05-0.1 mg.m-3. The higher concentrations can be observed during early spring bloom (February to April) with peaks of up to 5 mg.m-3. Concentrations between 0.1 and 0.2 mg.m-3 characterize the other periods of the year (Antoine et.al., 2008a). BOUSSOLE site permanently presents Case 1 water characteristics.

BOUSSOLE measures upwards and downwards plane irradiance and nadir upwelling radiance (respectively E_u, E_d and L_u) at two depths as well as above surface solar irradiance (E_s). A full description of the theoretical work, practical design and construction, laboratory and *in situ* testing of the buoy, along with a description of the instrument suite and of some aspects of the data processing are presented by Antoine *et al.* (2008a). The main steps are as follows. $L_u(\lambda,0^-)$ is extrapolated for the shallowest measurements as a function of K_L (diffuse attenuation coefficient for the upwelling nadir radiance), θ_s and chlorophyll concentration. K_L is calculated for the two depths L_u measurements. $L_u(\lambda,0^-)$ is then corrected for instrument self-shading. From $L_u(\lambda,0^-)$, the $L_w(\lambda)$ is calculated through signal propagation across the air/sea interface. $\rho_w^{IS}(\lambda)$ can then be calculated after $E_s(\lambda)$ tilt correction.

3.4.2 The MOBY dataset

The Marine Optical BuoY (MOBY - Clark *et al.*, 2003) has been moored since 1996 in the vicinity of Hawaii and measures upwelling radiance $L_u(\lambda)$ and downwelling irradiance $E_d(\lambda)$ over the spectral range 340nm to 955nm with 0.5nm spectral resolution at 1, 5 and 9m depth. MOBY also measures the surface irradiance $E_s(\lambda)$ through a collector on top of the buoy. Full details on the MOBY system can be found in Clark *et al.* 2003. Data processing includes extrapolation of $L_u(\lambda,z)$ to $L_u(\lambda,0^-)$ through the computation of upwelling radiance attenuation coefficient from two measurements of $L_u(\lambda,z)$, nominally the two upper arms. $L_u(\lambda,0^-)$ can then be propagated across the air/sea interface to compute $L_w(\lambda)$. Although MOBY is primarily designed for the NASA sensors SeaWiFs and MODIS, the hyperspectral data are also processed for MERIS bands. MERMAID database make use of $L_w(\lambda)$ and $E_s(\lambda)$ measured at MOBY to compute $\rho_w^{IS}(\lambda)$. No tilt correction is accounted for in MOBY data processing.

3.4.3 Data matching and screening

We gather all MERIS 19x19 pixels box overpassing each site coordinates over the complete MERIS mission duration, which makes a total of 1077 and 900 macropixels for BOUSSOLE and MOBY respectively, that we process at Level 1 and Level 2. We then employ a nested box approach, by searching among macropixels with the less possible cloud, ice haze, high glint, and medium glint, finally keeping the 5x5 central pixels. This procedure has been developed and checked for the MERIS 3rd data reprocessing.

3.4.4 Correction of downwelling sun irradiance for the in situ water-leaving reflectance

In the computation of $\rho_w^{IS}(\lambda,i)$ using downwelling and upwelling irradiances the solar irradiance E_s is the one measured in situ by the instruments. To remove potential bias from this measurement a normalization using the irradiance E_s^{ME} computed through the MERIS L2 processing is done.

E_s^{ME} is computed using the solar flux, the solar angle, the gaseous transmittance, and the total downward transmittance computed while performing the atmospheric correction (i.e. defined by the aerosols selected through the Antoine and Morel (1999) procedure).

It follows that we use the MERIS-normalized in situ water-leaving reflectance defined by

$$\rho_w^{ISME}(\lambda,i) = \rho_w^{IS}(\lambda,i).\frac{E_s(\lambda,i)}{E_s^{ME}(\lambda,i)} \qquad (16)$$

3.4.5 Denormalization procedure for the in situ water-leaving reflectance

All in situ water-leaving reflectances come into a fully-normalized format, which means that the original measurements have been normalized to a zenith-illuminating / nadir-viewing geometry. For the comparisons with MERIS a denormalization procedure is used to transform the reflectance to that which would be measured in the acquisition geometry (both illuminating and viewing) of MERIS. The denormalization is pixel-based and uses the same algorithm as the normalization of MERIS water-leaving reflectances (MERIS ATBD 2.9).

3.5 Vicarious gains computation

Formulations (14) and (15) using (16) are applied on the datasets mentioned above on an individual basis. Per match-up the uncertainty is given using the combination of the in situ and MERIS uncertainties:

$$\sigma_g^2 = \left(\sigma_g^{IS}\right)^2 + \left(\sigma_g^{ME}\right)^2 \qquad (17)$$

In the lack of in situ measurements assessment of total uncertainty σ_g^{IS} is taken as 5% of $\rho_w^{IS}(\lambda,i)$. The MERIS uncertainty is taken as the dispersion within the collection of $\rho_w(\lambda,i)$ per match-up. Then the weight associated to an individual gain is

$$\omega(\lambda,i) = \frac{1}{\sigma_g(\lambda,i)} \qquad (18)$$

The higher the uncertainty, the lower the weight. The final gain is firstly computed per site using (4):

$$G(\lambda) = \frac{\sum_{i=1}^{N}\omega(\lambda,i)g(\lambda,i)}{\sum_{i=1}^{N}\omega(\lambda,i)}$$

with $g(\lambda, i)$ computed following (15).

The whole visible spectrum from the 412 nm band to the 753 nm band is covered. BOUSSOLE had no data available at 620 nm and from 709 nm upwards, therefore we rely on MOBY from 709 nm. The 620 nm band is a special case: a rough interpolation of BOUSSOLE gains is made for the computation of the final gains.

Gains are first obtained separately for both sites along with the corresponding number of selected match-ups, at 620 nm the number of match-ups for BOUSSOLE is taken as the mean of the numbers for 560 and 665 nm. Then a mean, weighted by the number of match-ups as weights per site, is done per wavelength. Results are displayed in Table 1 and summarized in Figure *3* along with the associated standard deviations.

Table 1: Averaged gains per site and number of matchups, Final gains and standard deviation

Band (nm)	Gains BOUSSOLE	N BOUSSOLE	Gains MOBY	N MOBY	Gains Final	Standard deviation
412	0.9810	42	0.9813	127	0.9812	0.0104
443	0.9785	95	0.9833	127	0.9812	0.0111
490	0.9848	114	0.9849	127	0.9849	0.0112
510	0.9853	115	0.9848	127	0.9850	0.0121
560	0.9850	116	0.9853	127	0.9851	0.0100
620	N/A	0	0.9932	127	0.9910	0.0087
665	0.9926	72	0.9921	127	0.9923	0.0077
681	0.9921	62	0.9911	127	0.9915	0.0076
709	N/A	0	0.9925	122	0.9925	0.0085
753	N/A	0	0.9968	110	0.9968	0.0038

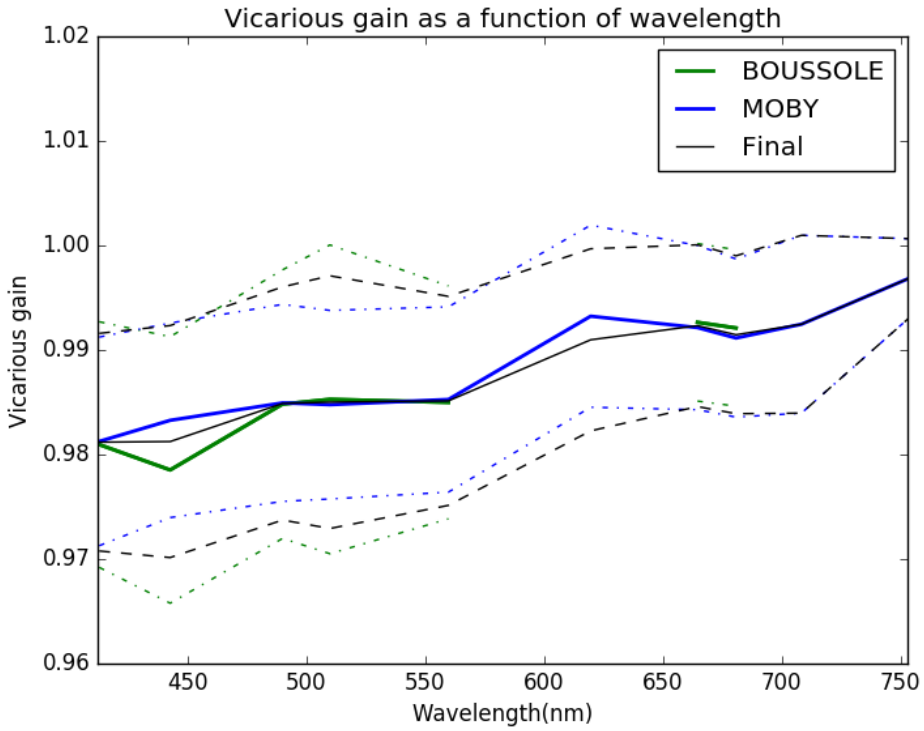

Figure 3: Vicarious gains computed over BOUSSOLE, MOBY, and final gains for MERIS 4th data reprocessing. Dashed lined represent standard deviation.

BOUSSOLE and MOBY gains are quite consistent, most differences occur at 443 nm. The overall spectral shape is quite linear, which is rather different to the gains of the 3rd data reprocessing. The dispersion is similar to that of the 3rd data reprocessing.

Applying the same methodology but using the formulation (14) of $g(\lambda, i)$ different sets of gains are obtained when choosing the atmospheric correction to be performed only using simulated atmospheres with reference pressure levels 1040, 1013.25, and 970 hPa. Results are displayed in Figure 4.

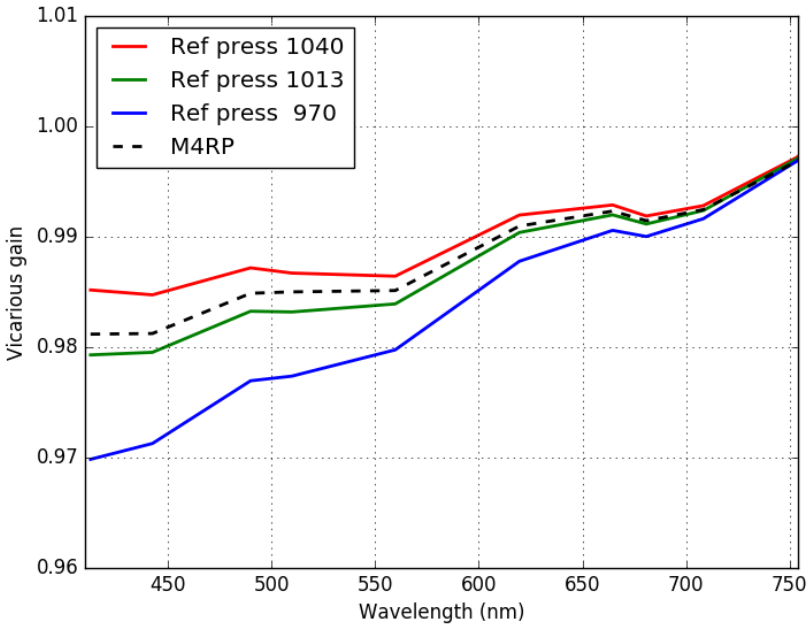

Figure 4: Final vicarious gains computed independently for selected pressure levels 1040, 1013.25, 970 hPa, compared to the nominal set of gains (dashed).

These results highlight the sensitivity of the atmospheric correction with the choice of the reference pressure of the radiative transfer simulations.

3.6 Validation on MERMAID matchups

Comparisons can be made between 2nd, 3rd and 4th data reprocessings with respect to the MERMAID database. Such database provides match-ups between in situ measurements and satellite water-leaving reflectances. Relative percent differences (used for the comparisons as figures from the 2nd and 3rd reprocessings are extracted from MERIS ATBD 2.24 issue 2011) are displayed in Figure *5* and Figure *6* for bands between 412 and 665 nm except 620 nm. Latest results from the 4th reprocessing are better (less bias) or at least in line (same bias and same dispersion) with previous reprocessings.

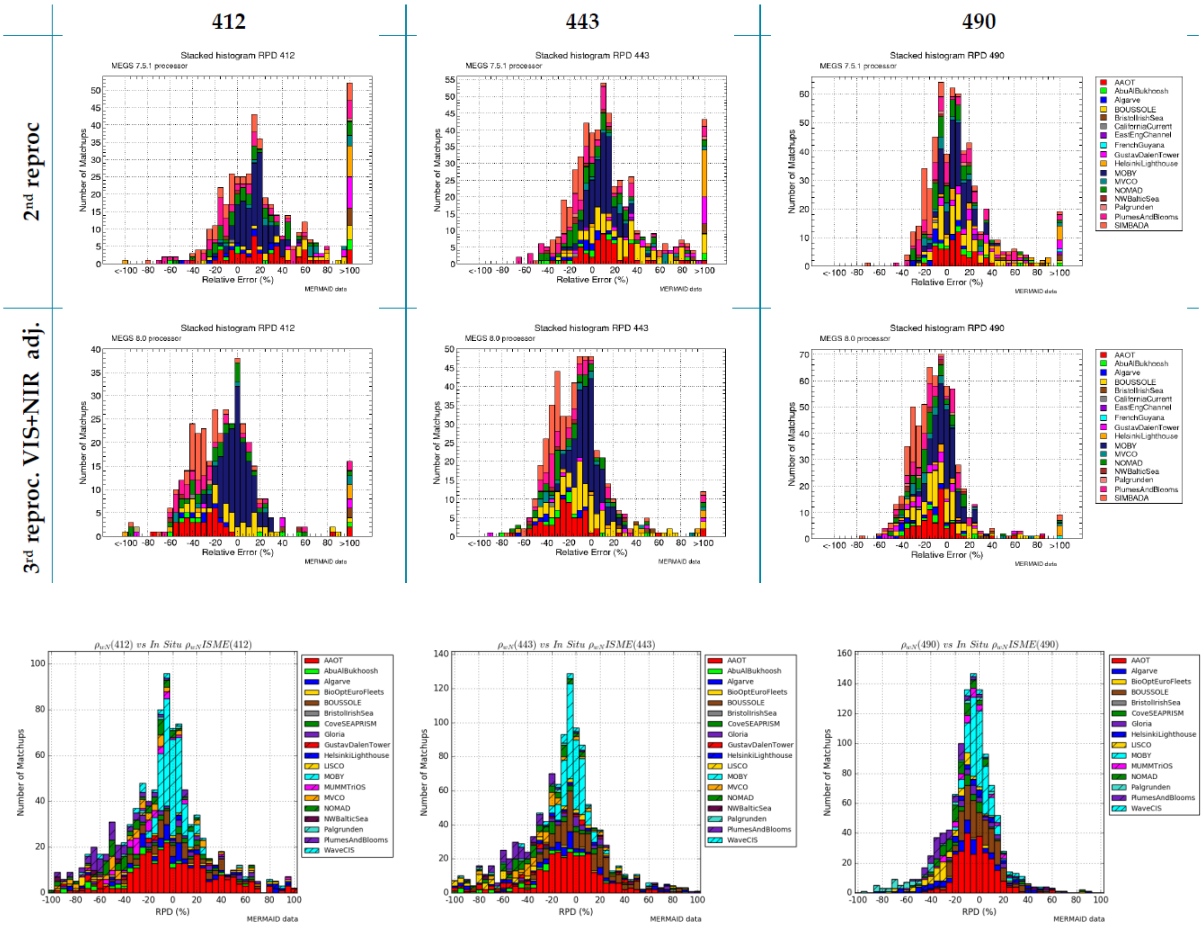

Figure 5: Relative percent difference in water-leaving reflectance between in situ and satellite (MERMAID) for wavebands 412, 443, 490 nm. From top to bottom: 2nd, 3rd, and 4th data reprocessings

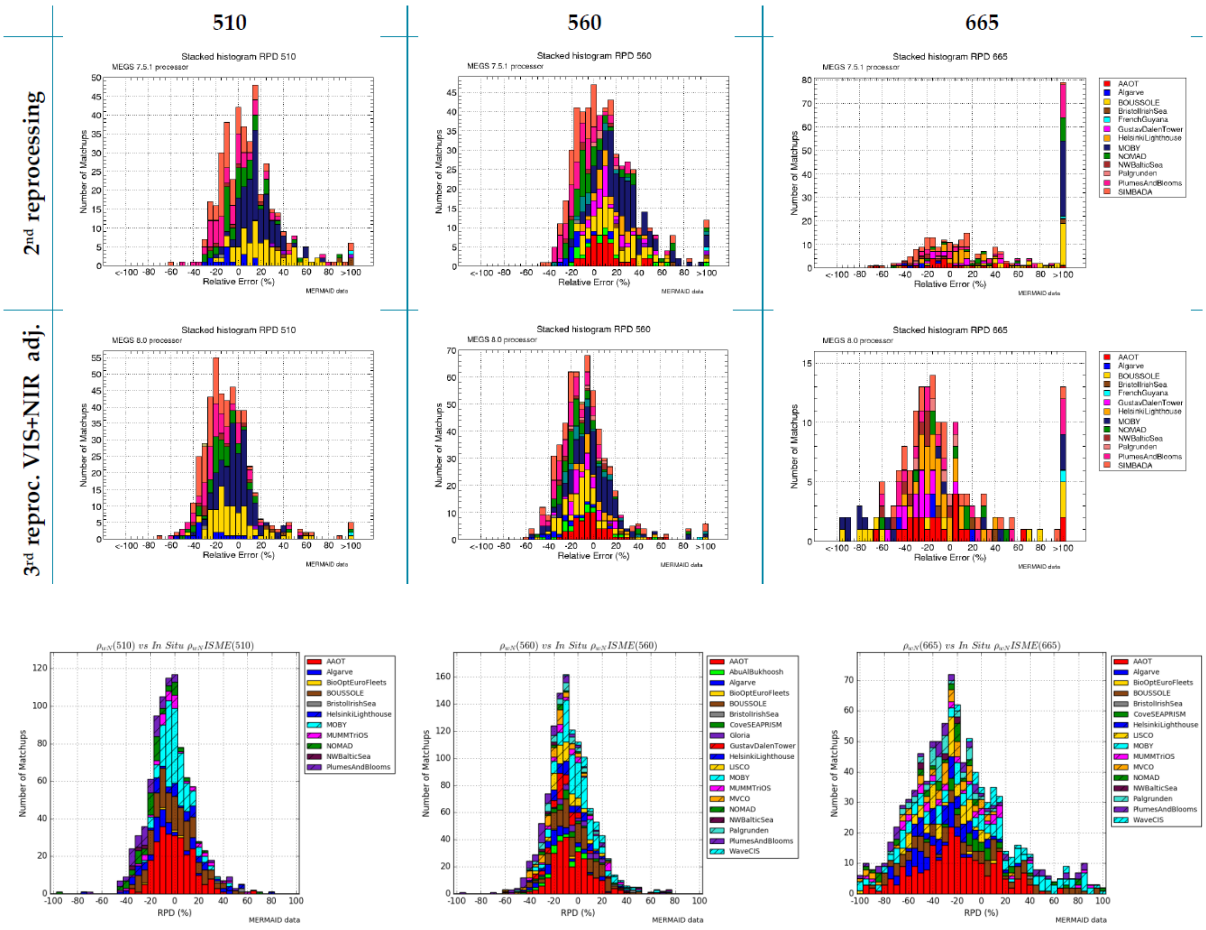

Figure 6: Relative percent difference in water-leaving reflectance between in situ and satellite (MERMAID) for wavebands 510, 560, 665 nm. From top to bottom: 2nd, 3rd, and 4th reprocessings.

Comparisons using either the individual gain formulation (14) or (15) can be made on the same basis. Both methods exhibit very similar results, for instance at 412 nm, which is shown through simple differences in Figure *7*. These results show that it is comparable to use one "mean" set of gains for any pressure branch of the atmospheric correction than to use specific sets of gains for each pressure branch. Question remains for high altitude water bodies: which approach would suit these cases ? We do not possess in situ measurements over high altitude waters to answer this question.

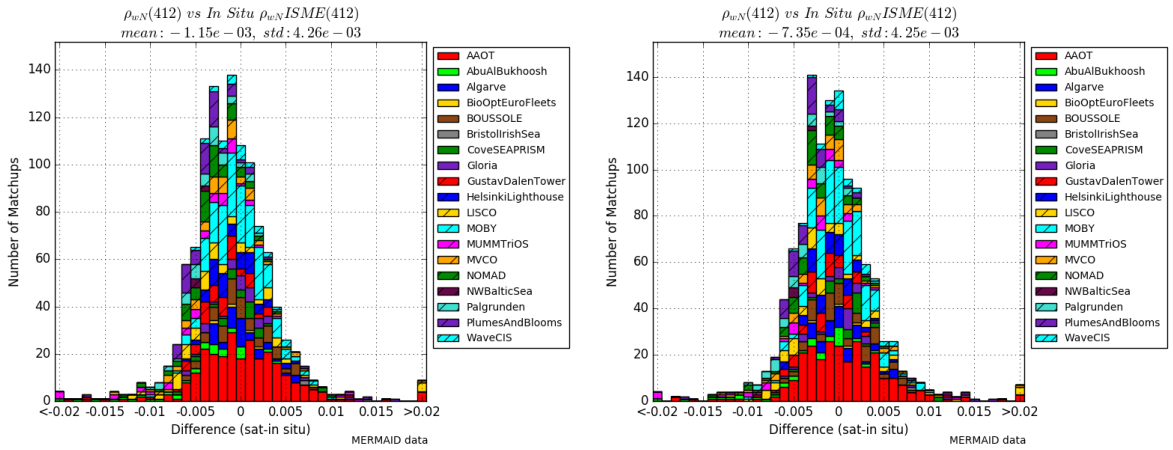

Figure 7: Difference in water-leaving reflectance between in situ and MERIS 4th reprocessing (MERMAID) for waveband 412 nm. Left: individual gain formulation (15), right: formulation (14).

4 References

Antoine, D. and A. Morel, 1998. Relative importance of multiple scattering by air molecules and aerosols in forming the atmospheric path radiance in the visible and near-infrared parts of the spectrum, Applied Optics Vol. 37, No. 12, 2245 – 2259.

Antoine, D. and A. Morel, 1999. A multiple scattering algorithm for atmospheric correction of remotely-sensed ocean colour (MERIS instrument) : principle and implementation for atmospheres carrying various aerosols including absorbing ones, International Journal of Remote Sensing, 20, 1875-1916.

Antoine, D., M. Chami, H. Claustre, F. D'Ortenzio, A. Morel, G. Bécu, B. Gentili, F. Louis, J. Ras, E. Roussier, A. J. Scott, D. Tailliez, S. B. Hooker, P. Guevel, J.-F. Desté, C. Dempsey and D. Adams, 2006. BOUSSOLE: a joint CNRS-INSU, ESA, CNES and NASA Ocean Color Calibration And Validation Activity. NASA Technical memorandum N° 2006 – 214147.

Antoine, D., P. Guevel, J.-F. Desté, G. Bécu, F. Louis, A.J. Scott and P. Bardey, 2008a. The «BOUSSOLE» buoy, a new transparent-to-swell taut mooring dedicated to marine optics: design, tests and performance at sea, Journal of Atmospheric and Oceanic Technology, 25, 968-989.

Antoine, D., F. D'Ortenzio, S. B. Hooker, G Bécu, B. Gentili, D. Tailliez, and A. J. Scott, 2008b. Assessment of uncertainty in the ocean reflectance determined by three satellite ocean color sensors (MERIS, SeaWiFS and MODIS-A) at an offshore site in the Mediterranean Sea (BOUSSOLE project), Journal of Geophysical Research, 113, C07013, doi:10.1029/2007JC004472.

Bailey, S. W., B. H. Hooker, D. Antoine, B. A. Franz and P. J. Werdell, 2008. Sources and assumption for the vicarious calibration of ocean color satellite observations, Applied Optics Vol. 47, No. 12, 2035 – 2045.

Clark, D. K., M. A. Yarborough, M. E. Feinholz, S. Flora, W. Broenkow, Y. S. Kim, B. C. Johnson, S. W. Brown, M. Yuen, and J. L. Mueller, 2003. MOBY, A Radiometric Buoy for Performance Monitoring and Vicarious Calibration of Satellite Ocean Colour Sensors: Measurements and Data Analysis Protocols. In Ocean Optics Protocols for Satellite Ocean Colour Sensor Validation, NASA Technical Memo. 2003-211621/Rev4, VolVI, 3-34 (Eds J. L. Muller, G. Fargion and C. McClain). Greenbelt, MD.: NASA/GSFC.

Cox, C. and W. Munk, 1954. Statistics of the sea surface derived from Sun glitter, Journal of Marine Research, 13, 198 – 227.

Cristina, S., P. Goela, J. I. Icely, A. Newton and B. Fragoso, 2009. Assessment of water-leaving reflectance of the oceanic and coastal waters using MERIS satellite products off the southwest coast of Portugal. Journal of Coastal Research Special Issue (56): 5.

Eplee, R. E. Jr., W. D. Robinson, S. W. Bailey, D. K. Clark, P. J. Werdell, M. Wang, R. A. Barnes, and C.R. McClain, 2001. Calibration of SeaWiFS. II. Vicarious techniques, Appl. Opt. 40, 6701–6718.

Franz, B. A., E. J. Ainsworth and S. W. Bailey, 2001. SeaWiFS, vicarious calibration: an alternative approach utilizing simultaneous *in situ* observations of oceanic and

atmospheric optical, properties, NASA Tech. Memo. 209982, National Aeronautics, and Space Administration, Goddard Space Flight Center, Greenbelt, MD.

Franz, B. A., S. W. Bailey, J. Werdell, Ch. McClain, 2007. Sensor-independent approach to the vicarious calibration. of satellite ocean color radiometryc. Applied Optics, Vol. 46, No. 22, 5068 – 5082.

Gordon, H. R and M. Wang, 1994. Retrieval of water-leaving radiance and aerosol optical thickness over the oceans with SeaWiFS: a preliminary algorithm, Appl. Opt. 33, 443 – 452.

Gordon, H. R., 1997. Atmospheric correction of ocean color imagery in the Earth observing system era, J. Geophys. Res. 102D, 17081 – 17106.

Gordon, H. R., 1998. In-orbit calibration strategy for ocean color sensors, Remote Sens. Environ. 63, 265 – 278.

Holben, B. N., T. F. Eck, I. Slutker, D. Tanré, J. P. Buis, A. Setzer, E. Vermote, J. A. Reagan, Y. J. Kaufman, T. Nakajima, F. Lavenu, I. Jankowiak and A. Smirnov, 1998. AERONET – A federated instrument network and data archive for aerosol characterisation, Remote Sens. Environ. 66, 1 – 16.

Hooker, S. B. and C. R. McClain, 2000. The calibration and valida-tion of SeaWiFS data, Prog. Oceanogr. 45, 427 – 465.

Hooker, S. B., W. E. Esaias, G. C. Feldman, W. W. Gregg and C. R. McClain, 1992. An overview of SeaWiFS and ocean color, NASA Tech. Memo. 104566, National Aeronautics and Space Administration, Goddard Space Flight Center, Greenbelt, MD.

Kneubühler, M., M. Schaepman, K. Thome, F. Baret, A. Müller, 2002. Calibration and validation of ENVISAT MERIS part 1: vicarious calibration at Rail Road Valley Playa (NV). Proceeding of the Envisat Validation Workshop 9-13 December 2002, ESRIN, Frascati, Italy.

Kratzer, S., C. Brockmann and G. F. Moore, 2008. Using MERIS full resolution data (300 m spatial resolution) to monitor coastal waters– a case study from Himmerfjärden, a fjord-like bay in the north-western Baltic Sea. Remote Sensing of the Environment 112(5): 2284-2300.

Loisel, H., X. Mériaux, A. Poteau, L. F. Artigas, B. Lubac, A. Gardel, J. Caillaud, and S. Lesourd, 2007. Analyze of the inherent optical properties of French Guiana coastal waters for remote sensing applications. Journal of Coastal Research SI 56 (Proceedings of the 10th International Coastal Symposium), 1532 – 1536.

Lubac B. and H. Loisel, 2007. Variability and classification of remote sensing reflectance spectra in the Eastern English Channel and southern North Sea. Remote Sensing of Environment 110, 45-58.

Mélin F. and G. Zibordi, 2010. Vicarious calibration of satellite ocean color sensors at two coastal sites, Applied Optics, vol 49 n°5, pp798 – 810.

MERIS ATBD 2.6, issue TBD.

MERIS ATBD 2.9, issue Jul 2011. Pigment index retrieval in case 1 waters.

MERIS ATBD 2.13, issue Jul 2011. Sun Glint Flag Algorithm.

MERIS ATBD 2.24, issue Sep 2011. Vicarious adjustment of the MERIS Ocean Colour Radiometry.

Rast, M. and J.-L. Bezy, 1999. The ESA Medium Resolution Imaging Spectrometer MERIS: A review of the instrument and its mission. International Journal of Remote Sensing, 20(9), 1681 − 1702.

Ruddick, K. G., V. De Cauwer, Y. Park and G. Moore, 2006. Seaborne measurements of near infrared water-leaving reflectance - the similarity spectrum for turbid waters. Limnology and Oceanography 51(2): 1167-1179.

Santer, R., and F. Zagolski, 2017. Technical note on pressure adjustment. TBD

Werdell, P. J. and S. W. Bailey, 2005. An improved bio-optical data set for ocean color algorithm development and satellite data product validation. Remote Sensing of Environment, 98(1), 122-140.

Zibordi, G., F. Mélin, and J.-F. Berthon, 2006. Comparison of SeaWiFS, MODIS and MERIS radiometric product at a coastal site, Geophysical research letters, vol 33, L06617, doi: 10.1029/2006GL025778

G. Zibordi, B. Holben, I. Slutsker, D. Giles, D. D'Alimonte, F. Mélin, J.-F. Berthon, D. Vandemark, H. Feng, G. Schuster, B. Fabbri, S. Kaitala, J. Seppälä, 2009a. AERONET-OC: a network for the validation of Ocean Color primary radiometric products. Journal of Atmospheric and Oceanic Technology, 26, 1634-1651.

G. Zibordi, J.-F.Berthon, F.Mélin, D. D'Alimonte and S.Kaitala, 2009b. Validation of satellite ocean color primary products at optically complex coastal sites: northern Adriatic Sea, northern Baltic Proper and Gulf of Finland. Remote Sensing of Environment, 113, 2574-2591.

End of Document